



D1.5 – Demonstrate the time course of development of cross- modal plasticity for sonification

## TABLE OF CONTENTS

<b>INTRODUCTION .....</b>	<b>3</b>
<b>RESULTS .....</b>	<b>6</b>
<b>CONCLUSIONS.....</b>	<b>15</b>
<b>REFERENCES .....</b>	<b>15</b>

## Introduction

Early onset blindness is associated with superior spatial hearing skills in the azimuthal plane, including enhanced localization acuity in the auditory periphery (1-4), and more accurate monaural sound localization (5-7). The latter results sparked the hypothesis that some early blind individuals may learn to use spectral, monaural cues for sound localization in the horizontal plane, possibly at the cost of their spatial acuity in the vertical plane (7).

At the cortical level, early visual deprivation induces widespread cross-modal reorganization. Specifically, neuroimaging studies investigating cross-modal plasticity show that early blind humans recruit dorsal extrastriate areas during sound localization tasks, including the right occipital cortex (8), the right middle occipital gyrus (9, 10), and the right cuneus (9). In addition, monaural sound localization performance and neural activity in dorsal extrastriate areas are correlated in blind individuals (6, 11). A virtual lesion study supports the notion that these areas are indeed functionally relevant for auditory localization in EB (12). It was therefore argued that extrastriate visual areas – which are part of the visual “where” pathway – preserve their functional specialization for spatial processing even when the input modality changes from visual to auditory (9, 10).

Relatively few studies have investigated auditory intra-modal plasticity following the loss or absence of vision. Further, although some studies investigated auditory intra-modal functional plasticity for the processing of sound frequency (tonotopy) and auditory motion (11-16), there are almost none that focused on cerebral changes in sound location processing within the auditory cortex of blind humans (see only 17). It therefore remains unclear how early visual deprivation may alter sound location processing in auditory cortex, how such intra-modal plasticity relates to the cross-modal activation of occipital areas, and whether the recently hypothesized superior processing of monaural, spectral cues is reflected in neural activity patterns.

The present study investigated intra- and cross-modal changes in CB for azimuthal sound location processing. We compared blood-oxygenation level dependent (BOLD) signals measured in twelve congenitally blind (CB) participants (mean age: 42.3 years; standard deviation [SD]: 9.1 years; range: 27 - 54 years) and twelve age-matched sighted controls (SC; mean age: 39.4 years; SD: 8.8 years; range: 26 – 53 years; see Table S1 and SI Materials and Methods for details). We employed a phase-encoding fMRI paradigm in which participants listened to subject-specific binaural recordings of sounds moving smoothly through the azimuthal plane (360°) at three intensity levels (see also 18).

## METHODS

### Participants

Twelve sighted (mean age = 39.4 years, standard deviation [SD] = 8.8 years, range = 26 – 53 years) and twelve congenitally blind individuals (mean age = 42.3 [9.1] years, range = 27 – 54 years; Table S1) volunteered to participate in the study. Hearing levels were screened for all participants with pure tone audiometry at 0.5, 1, 2, 4 and 6 kHz. Participants reported no history of neurological disorders.

## Binaural recording set-up

Participants were seated in a chair and microphones were placed in their ear canals (OKM II Classic Microphone, Soundman, Germany; sampling rate = 44.1kHz). The chair was positioned in the middle of a normal room (internal volume = 95m<sup>3</sup>) with walls and ceiling of gypsum board and a floor of wood with a thin carpet on top. Sounds were played through a 3D sound system with 22 loudspeakers in a spherical set-up in the far field (12 speakers in the horizontal plane at the elevation of the interaural axis and a distance of 2.4m from the participant). We positioned sounds in the acoustic 3D environment with the virtual reality software Vizard (Worldviz, Santa Barbara, United States). Participants were monitored with a video camera attached to the wall to ensure that no head movements were made during the recordings. Sounds were presented at 75dB SPL.

## Data acquisition and preprocessing

Functional and anatomical data were collected with a Siemens whole body MRI scanner at the Scannexus MRI scanning facilities (Maastricht, [www.scannexus.nl](http://www.scannexus.nl)) with a Siemens Prisma 3.0T at 2mm<sup>3</sup> and 1mm<sup>3</sup> isotropic voxel resolution respectively. Data were recorded with a standard T<sub>2</sub>\*-weighted echo planar imaging sequence covering the temporal cortex as well as parts of the parietal, occipital and frontal cortex [echo time (TE) = 30ms; repetition time (TR) = 2000ms; flip angle = 90°; matrix size = 100 x 100; voxel size 2 x 2 x 2 mm<sup>3</sup>; number of slices = 32]. Anatomical data was obtained with a T<sub>1</sub>-weighted MPRAGE sequence with the following parameters: TE = 2,17ms; TR = 2250ms; voxel size 1 x 1 x 1 mm<sup>3</sup>; matrix size = 192 x 256 x 256.

During the fMRI session, audio recordings were presented with MR-compatible earphones (Sensimetrics Corporation, [www.sens.com](http://www.sens.com)) at three intensity levels (spaced 10dB apart). Participants were instructed to listen attentively to the location of the sounds. Sound level was scaled individually for each participant such that the lowest intensity was comfortable and audible on top of the scanner noise. Sound intensity was furthermore equalized between the 250 – 700Hz and the 500 – 1400Hz frequency range (subjective perception). In total, there were 24 conditions (i.e. two frequency levels, two starting points, two rotation directions, three intensity levels). Each condition was presented 3 times, resulting in 72 trials in total. Trials were presented in 6 runs of 12 trials each in which each run presented sounds of one intensity only (soft, medium or loud). The order of runs was randomized and counterbalanced across participants. Starting position and rotation direction of the sounds were counterbalanced and randomized both within and across runs.

Preprocessing of functional data consisted of head motion correction (trilinear/sinc interpolation, the first volume of the first run functioned as reference volume for alignment), inter-scan slice-time correction (sinc interpolation), linear drifts removal and temporal high-pass filtering (threshold at 7 cycles per run). Functional data were mildly smoothed (3mm kernel). We coregistered functional data to the T<sub>1</sub>-weighted images of each individual, and sinc-interpolated to 3D Talairach space at 2mm<sup>3</sup> resolution (46). Gray/white matter borders were defined with the automatic segmentation procedure of

BrainVoyager QX and complemented with manual improvements. Optimum co-registration of cortical surface across participants was achieved with cortex based alignment (CBA) of the participants' cortical surface reconstructions (47). For the detailed analysis of the auditory cortex in the context of the population coding model, we performed the CBA constrained by an anatomical mask of Heschl's gyrus (48). This procedure is similar to the functional CBA procedure (49): an anatomical definition of a region of interest is used to optimize the local realignment of this region rather than a globally realigning the entire cortex. Functional data were then projected from volume space to surface space by creating mesh time courses from volume time courses. A value was obtained for each vertex of the cortex mesh by sampling (trilinear interpolation) and computing the average value of that location in the volume time course from the gray/white matter boundary up to 4mm into the gray matter (toward the pial surface).

### Waveshape Index

We estimated a RFX GLM with two predictors (one modeling a sustained response and the other modeling a phasic response) to evaluate which brain regions exhibited increased activation during presentation of spatialized sounds (23,24). The Waveshape Index reflects the normalized difference between the beta weights of the sustained predictor and the phasic predictor (Equation 1; 24).

$$WI = \frac{\beta_{sustained-} - \beta_{phasic}}{\beta_{sustained+} + \beta_{phasic}} \quad \text{Equation 1}$$

### Analyses of response azimuth functions (RAFTs)

We started the RAFT analysis with an estimation of the time-to-peak (TTP) of the hemodynamic response function (HRF) for each participant (18). This was done to ensure that inter-individual differences in the shape of the HRF do not affect our results. We estimated 3 General Linear Models (GLMs) with double gamma HRF functions (50) for each functional run with TTPs ranging from 4 to 8s, in steps of 2s. The optimal TTP value for each participant was selected based on the number of significantly active voxels (*auditory > baseline*,  $p < .05$ , Bonferroni corrected) resulting from each TTP value and the average t value across these voxels. For most participants ( $n = 11$  for SC,  $n = 9$  for CB), the optimal time-to-peak was 6 seconds, for some this was 4 seconds ( $n = 1$  for SC,  $n = 2$  for CB) or 8 seconds ( $n = 1$  for CB).

As mentioned in the main text, we constructed RAFTs with the beta estimates for each azimuth location as estimated with a Finite Impulse Response (FIR) deconvolution analysis (26). The best location of a vertex was then defined based on the RAFT as the vector sum of the azimuths eliciting a peak response in the RAFT (75% or more of the maximum response of that vertex (51, 52). The location of peak-slope was defined as the maxima and minima of the spatial derivative of the RAFT (52). Finally, we quantified spatial tuning width for each vertex as the equivalent rectangular receptive field (ERRF) width (18, 27). To compute, the area under the RAFT was transformed into a rectangle with height equivalent to the peak response in the RAFT and an equivalent area. The resulting ERRF

width does not provide information on absolute tuning width, yet it does enable the comparison of spatial selectivity across conditions.

Note that we discarded from the analyses above those auditory responsive vertices that exhibited high frequency oscillations as these likely reflect noise rather than neural responses to the stimuli. We therefore estimated the Fourier transform of each RAF and excluded those having more than 20% of total power in high frequency bands (average proportion of vertices discarded = 13.5% [SD = 8.4%]).

### **Assessing cortical sensitivity to binaural spatial cues**

As described in the main text, we estimated a RFX GLM with ‘binaural difference predictors’ to identify the regions responsive to binaural spatial cues. Note that we did not compute ITDs here as we previously showed that predictors based on the ITD and ILD information in these stimuli are highly correlated, rendering the ITD predictor redundant (18). The design matrix of the GLM also included binaural sum predictors for each sound to explain the variance due to the general neural response to the sound independent of sound position. We computed the binaural sum predictor by convolving the sum in power (root mean square; RMS) in the left and right ear of the recording with the HRF (18).

## **Results**

### **General processing of spatialized sounds**

We measured 3T fMRI responses while participants listened to spatialized stimuli that consisted of frequency modulated (FM) sweeps. Frequency decreased exponentially at a rate of 2.5 octaves/s and sweeps (0.45s duration) were repeated at a rate of 2Hz while moving smoothly through the horizontal plane. Stimuli were presented at three different intensity levels spaced 10dB apart, and in two frequency conditions: either spanning a frequency range of 250 – 700Hz, or of 500 – 1400Hz. Each stimulus started with a stationary period of 10s at  $-90^\circ$  or  $+90^\circ$ , followed by a full circle around the head of the participant in 20s (rotation speed =  $18^\circ/s$ ), and concluded with another stationary period of 10s at the same location as the starting position (either  $-90^\circ$  or  $+90^\circ$ ). This resulted in a total stimulus duration of 40s. All stimuli were presented at zero elevation relative to the listener, and starting position and rotation direction were randomized and counterbalanced within and across runs. Onset and offset of stimuli were ramped with a 50ms linear slope. Finally, stimuli were spatialized with subject-specific binaural recordings to maximize the availability of spatial cues in the scanner (*SI Materials and Methods*). This procedure resulted in realistic, well localizable auditory stimuli. We confirmed that participants were able to localize stimuli with verbal reports of the sound azimuth trajectory for each participant. Reports were accurate for all participants apart from some front-back reversals, which are commonly observed in human sound localization (19, 20).

Stimuli were then presented in a phase-encoding stimulation paradigm (18) similar to those used to map visual space in the occipital cortex (21) and the tonotopic organization in auditory cortex (22). This paradigm enables the mapping of acoustic azimuth sensitivity in the auditory cortex and offers the possibility to investigate whether other cortical areas or networks are activated during the processing of azimuthal locations in CB.

To examine the general processing of spatialized sounds, we estimated a random effects general linear model (RFX GLM) with two predictors per trial: one modeling a sustained BOLD response, and one modeling a phasic BOLD response (23, 24). Figure 1 shows the functional activation maps resulting from the contrast *Auditory Stimulation > Baseline*. The auditory cortex exhibited increased activation in response to spatialized sounds in both CB and SC, although more extensively in SC. Activated regions included Heschl's gyrus (HG), Heschl's sulcus (HS), planum temporale (PT), planum polare (PP), and the superior temporal gyrus (STG). In addition, SC showed clusters of activation bilaterally in the inferior parietal sulcus (IPS), corpus callosum sulcus (CSS), superior parietal lobule (SPL), and left parieto-occipital sulcus (POS). In CB we observed clusters in bilateral POS, and in the right cuneus. At a more liberal threshold, we also observed clusters of activation in bilateral calcarine sulcus (CS) or POS (Figure 1, lower panel).

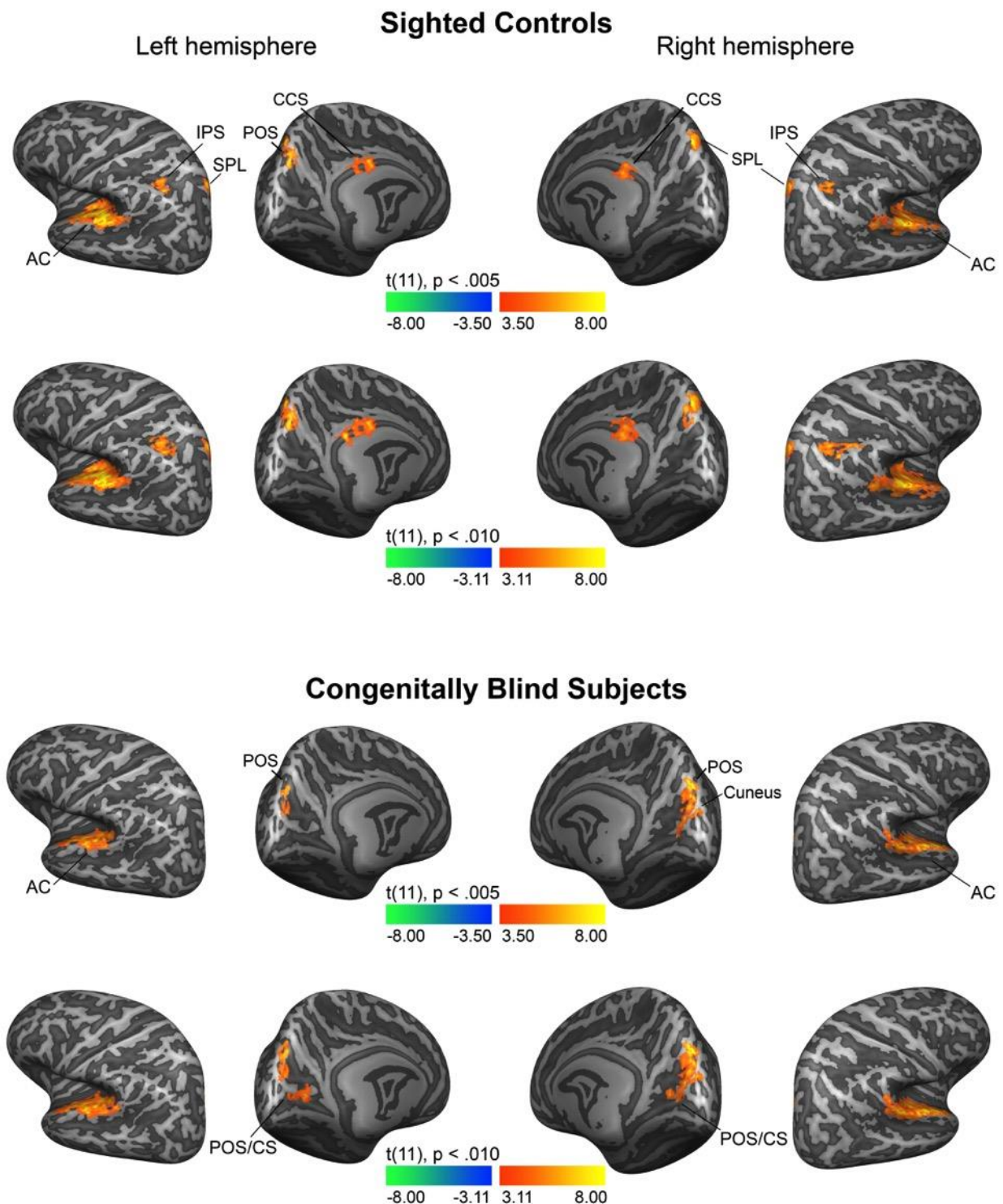


**Figure 1. Functional activation in response to spatialized sounds in sighted controls and in congenitally blind subjects.** Maps show the results of the within-group RFX GLMs (contrasting *Auditory stimulation* versus *Baseline*) projected on the group averaged cortical surface. For each participant group, maps at two levels of cluster size correction are displayed (initial threshold  $p < 0.005$  in the top row for each participant group, and initial threshold  $p < 0.010$  in the bottom row for each participant group). Cluster size thresholds were computed with 3000 iterations for all maps, and had a final threshold of  $p < 0.05$ . AC = auditory cortex. IPS = inferior parietal sulcus. POS = parieto-occipital sulcus. CCS = corpus callosum sulcus. SPL = superior parietal lobule. CS = calcarine sulcus.

A between-group comparison using the summary statistics approach (25) showed that CB activate several occipital areas more strongly than SC during auditory processing. Specifically, we observed clusters in bilateral POS and cuneus (Figure 2, top row). Using a more liberal threshold of  $p < 0.05$  (cluster size corrected for multiple comparisons) revealed additional clusters of increased activation in the retrosplenial cortex (RSC) in the left hemisphere, and a cluster in the right middle occipital gyrus (MOG). We further observed a cluster showing decreased activity in CB compared to SC in left medial auditory cortex (Figure 2, bottom row).

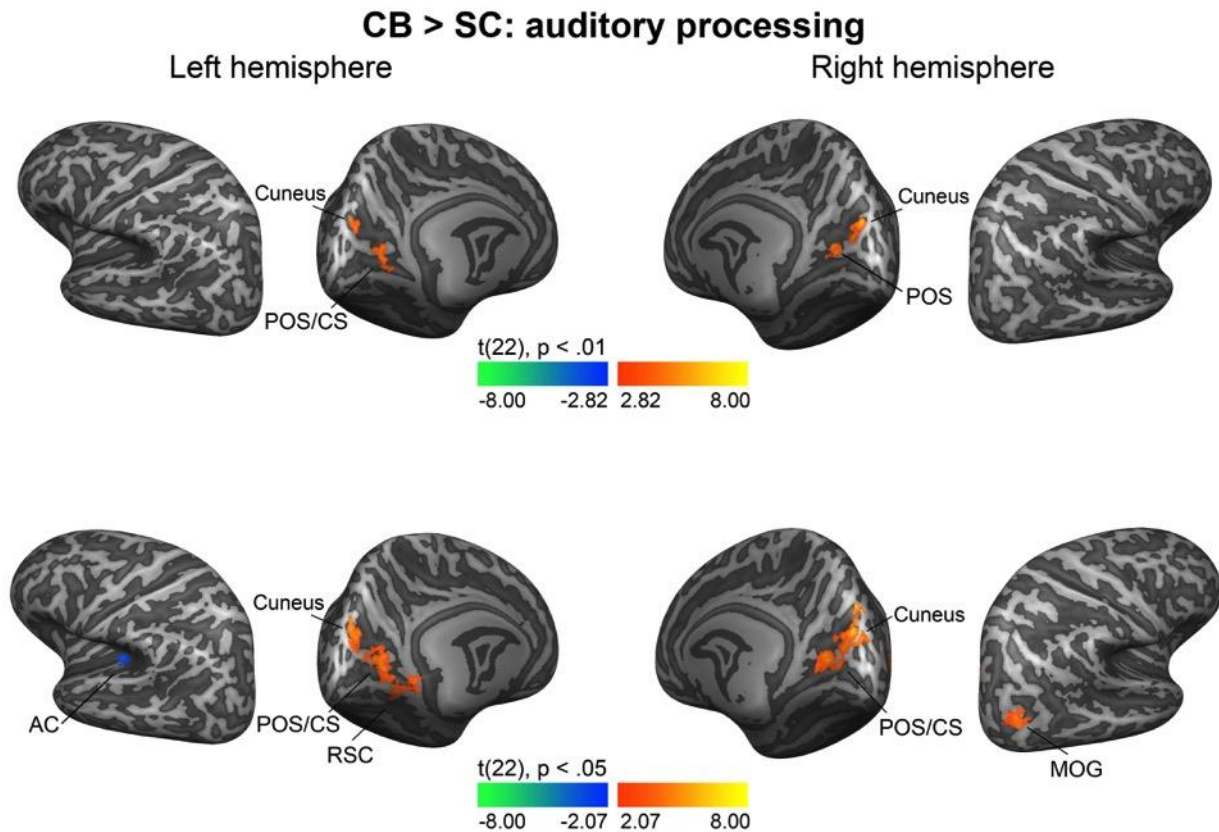


**Figure 2. Group differences in functional activation between congenitally blind subjects and sighted controls.** Maps show the result of a mixed effects model testing for group differences in functional activation between CB and SC. The top row shows maps thresholded at  $p < 0.01$  (cluster size corrected for multiple comparisons, 3000 iterations); the bottom row displays maps thresholded more liberally at  $p < 0.05$  (cluster size corrected for multiple comparisons, 3000 iterations). AC = auditory cortex. CS = calcarine sulcus. MOG = middle occipital gyrus. POS = parieto-occipital sulcus. pCC = posterior cingulate sulcus. SPL = superior parietal lobule.

We then investigated whether the shape of the BOLD response in the activated occipital areas of CB is similar to that in the activated auditory areas in CB and SC. Specifically, we quantified the contribution of the sustained and phasic response components to the overall BOLD response by computing a *Waveshape Index* (WI; 23, 24) for each auditory responsive vertex in a participant (fixed

effects [FFX] GLM, contrast *auditory stimulation* > *baseline*;  $p < 0.005$ , cluster size corrected). The WI is computed as the normalized difference between the estimated beta for the sustained and phasic predictors. The resulting average WI was positive in the auditory cortex of both blind and sighted participants, indicating that the BOLD response was mainly driven by a sustained component in this cortical region (average WI for CB [standard deviation] = 0.27 [0.22]; average WI for SC: 0.23 [0.22]). In contrast, WIs in the occipital cortex of CB were more variable. For some participants, the average WI was negative while for some others positive (average WI 0.06 [1.11]). This indicates that the shape of the BOLD response to long-duration, spatialized sounds in the occipital cortex varies considerably between individuals and that the occipital BOLD response has a more phasic nature than the BOLD response in auditory cortex.

### **Spatial tuning width is more robust to increasing sound level in CB than in SC**

To test for differences in cortical spatial tuning between SC and CB, we constructed a response azimuth function (RAF) for each responsive vertex in auditory cortex (fixed effects [FFX] GLM, contrast *Auditory Stimulation* > *baseline*;  $p < 0.005$ , cluster size corrected). RAFs consisted of ten beta estimates, one for each azimuth location (spaced  $36^\circ$  apart) as estimated with a Finite Impulse Response (FIR) deconvolution analysis (26). RAFs were mildly smoothed with a moving average window (width: three azimuthal locations, weights [0.2 0.6 0.2]). Trials were pooled across rotation direction. From the RAFs we inferred for each voxel its best location and peak-slope location. The latter refers to the azimuth position with the highest modulation rate. In addition, we computed for each vertex the equivalent rectangular receptive field (ERRF) width as a relative measure of spatial selectivity. The ERRF reflects the ratio between the peak response and the integral of the RAF (18, 27; Materials and Methods).

The RAF analysis showed that although there was no difference in spatial tuning width between SC and CB when averaged across the three sound intensity levels (Wilcoxon rank-sum tests,  $p > 0.05$  for both frequency ranges), tuning width was robust to increasing sound level in CB but not in SC. Specifically, spatial tuning broadened significantly with increasing sound level in SC for stimuli in the 250 – 700 Hz (Figure 3 B, *left*, Friedman test,  $\chi^2(22) = 14$ ,  $p = 0.004$ ; reported  $p$  values in this paragraph have been Bonferroni corrected for multiple comparisons), as well as in the 500 – 1400 Hz range (Figure 3 B, *right*,  $\chi^2(22) = 13.5$ ,  $p = 0.005$ ). In contrast, although spatial tuning width for sounds in the 500 – 1400 Hz range showed a similar pattern in CB (Figure 3 C, *right*), spatial tuning did not broaden significantly with higher sound intensities for sounds in the 250 – 700 Hz range (Figure 3 C, *left*,  $\chi^2(22) = 4.67$ ;  $p = 0.39$ ) or for sounds in the 500 – 1400 Hz range ( $\chi^2(22) = 8.17$ ;  $p = 0.07$ ).

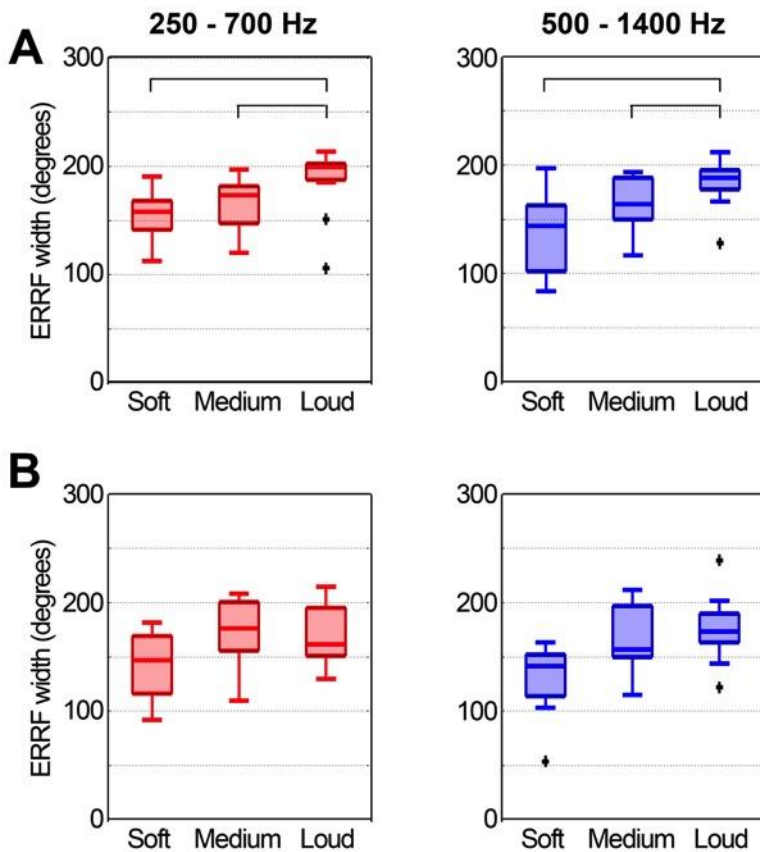


**Figure 3. Spatial tuning width in CB is more robust to sound level variations.** Box-plots of average ERRF width per participant for each sound intensity within a frequency condition. (A) shows box plots for sighted controls, (B) for congenitally blind participants. Red boxes indicate the 250 – 700Hz frequency range, blue boxes the 500 – 1400Hz range. For each box, the central line indicates the median, the edges the 25<sup>th</sup> and 75<sup>th</sup> percentiles, and the whiskers indicate the range of values (excluding outliers). Outliers are indicated as black crosses above or below the box. Black horizontal lines indicate a significant difference between conditions as assessed with post-hoc comparisons ( $p < 0.05$ , Tukey correction for multiple comparisons).

Azimuth sampling, however, was similar for CB and SC. That is, for both participant groups the best location of the majority of auditory responsive vertices was in the contralateral hemifield (~47%), with smaller proportions responding maximally to ipsilateral space (~32%) or midline locations (~21%; see Table S2 for details). The distribution of peak-slope locations was also similar for CB and SC: for the majority of vertices, the peak-slope was to the interaural midline.

### The auditory cortex of CB is less sensitive to binaural spatial cues

Next we investigated whether early visual deprivation affects sound azimuth sensitivity based on binaural spatial cues in the auditory cortex. To this end, we used a regression analysis with ‘azimuth’ predictors that were constructed individually for each participant. Specifically, even though the azimuth trajectory was known, we constructed azimuth predictors based on interaural level differences (ILD) that were inferred from the subject-specific binaural recordings to directly compare

the neural response to the perceived ILD. We computed the ILD azimuth predictor as the arithmetic difference between the root mean square (RMS) power in each channel, convolved with a double-gamma hemodynamic response predictor (SI Materials and Methods; see also 18). We then employed these predictors to estimate a RFX GLM within each group of participants (SC and CB) to identify regions that are modulated by binaural spatial cues, that is, regions sensitive to azimuth based on binaural differences (contrasting *Binaural Difference* > *Baseline*).

We estimated the GLMs three times, each time on a sub set of the data. Specifically, data of two sound intensity levels only were included per GLM, and we used the remaining data at a later stage as an independent data set to decode sound azimuth position. Figure 4 shows the resulting activation maps (thresholded at  $p < 0.005$  and cluster size corrected for multiple comparisons, 3000 iterations). Regions sensitive to sound azimuth based on binaural cues – that is, regions modulated by ILD – are present in the auditory cortex of SC for stimuli in both frequency ranges and at all sound intensity levels (red areas in Figure 4). In contrast, in CB we observed these regions for a few combinations of sound frequency and intensity only, and these regions were mostly located in the right hemisphere (green areas in Figure 4). We did not observe any regions sensitive to binaural spatial cues in the occipital or parietal cortices of CB either.

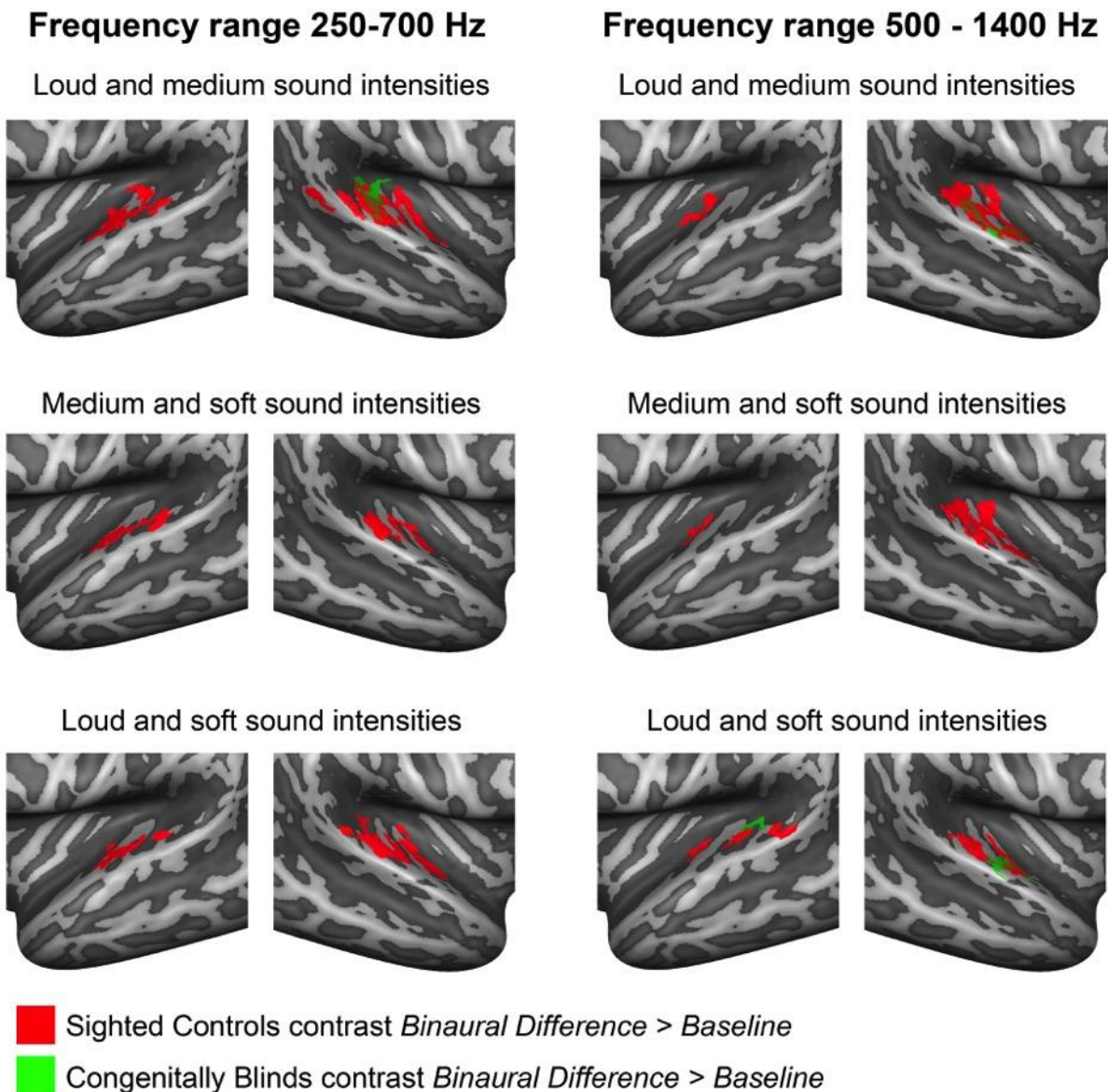


**Figure 4. Cortical areas modulated by binaural spatial cues in CB and SC.** Maps show the result of the RFX GLMs estimated with the binaural sum and binaural difference predictors, contrasting *Binaural Difference (ILD)* versus *Baseline* for SC (red colors) and CB (green colors). That is, colored regions exhibit spatial sensitivity based on binaural spatial cues. GLMs were estimated based on a subset of the data: data of two sound intensities only was included in each GLM estimation (see headings above maps). Maps were thresholded at  $p < 0.005$  and cluster size corrected for multiple comparisons (3000 iterations,  $p < 0.05$ ). All regions responded maximally to contralateral sound locations.

To conclude, we assessed whether detailed information on azimuth position is represented in these spatially sensitive regions by decoding the sound azimuth trajectory from the BOLD response in these regions. Specifically, for the spatially sensitive regions that were revealed by the three RFX GLMs estimated with binaural difference predictors on two sound level conditions, we decoded the sound trajectory from the BOLD response in these regions in the third sound level condition that was left out of the GLM estimation. This we did with two decoding models: a two-channel, opponent model, and a

local, one-channel model (18). For the two-channel opponent coding model, we computed azimuth estimates for each time point by calculating the difference in average BOLD response within the spatially sensitive regions in each hemisphere (that is, the difference between the population responses in each hemisphere). For the local, one-channel model we used the average BOLD response of the spatially sensitive region in one hemisphere only. Reconstructed sound azimuth trajectories were mildly smoothed in the temporal domain (simple moving average, window spanning three time points).

Figure 5 shows that for SC, the correlation between the reconstructed and the actual sound azimuth trajectory was high for the opponent coding model. As expected, the one-channel model performed less well (see also 18). For CB, we could reconstruct the sound azimuth trajectory with the opponent-coding model for only one condition (500 – 1400Hz, medium sound intensity) due to the absence of spatially sensitive regions in the other GLMs (Figure 4). The results show that for CB, the opponent model could accurately reconstruct the azimuth trajectory for the stimuli in this condition as well, and the estimates were more accurate than those for the one-channel model (Figure 5, note that the scatterplot figure only shows the correlation values for the condition for which the two-channel, opponent coding model could be estimated as well). However, the median correlation between the one-channel azimuth estimates and the actual azimuth trajectory across all conditions in which a spatially sensitive region was observed in at least one hemisphere in CB (see Figure 4), was lower in CB than in SC (median  $r = 0.529$  for CB and median  $r = 0.767$  for SC, Wilcoxon rank-sum test,  $p = 0.031$ ).

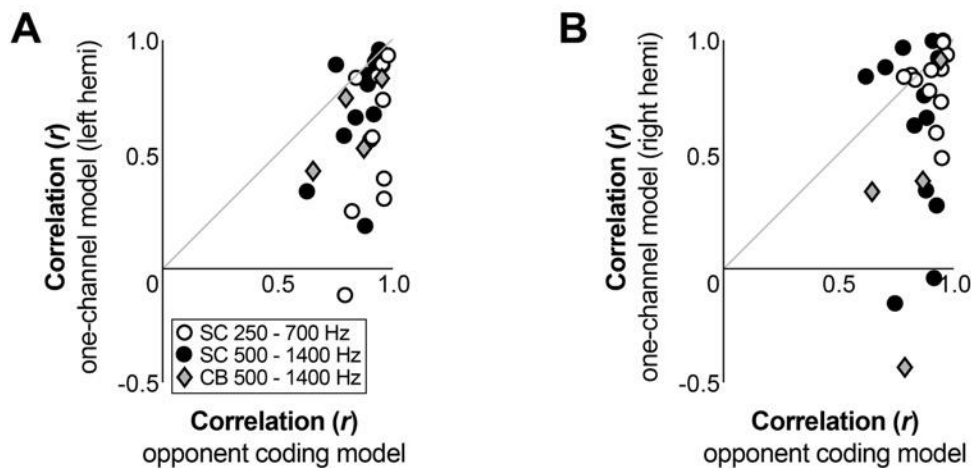


**Figure 5. Decoding sound azimuth from BOLD signals in the auditory cortex with a two-channel, opponent model and a local, one-channel model.** Scatter plots display the correlation between the azimuth position estimated with the opponent coding model and the actual sound azimuth position (x-axis), plotted against the correlation between the azimuth position estimated with the local, one-channel model (y-axis) in the left hemisphere (A) and right hemisphere (B). Circles represent the correlations for SC: white circles for sounds in the 250 – 700Hz frequency range, black circles for sounds in the 500 – 1400Hz range. Diamonds represent correlations for CB in the 500 – 1400 Hz frequency range (we did not observe bilateral channels in the 250 – 700Hz range). Each symbol represents the correlation for one condition within a frequency range (e.g. soft intensity, starting left, rotating clockwise; 12 conditions per frequency range). Symbols below the diagonal

indicate higher correlation values (that is, higher decoding accuracy) for the opponent coding model compared to the local, one-channel model.

## Conclusions

The present study demonstrates that congenital blindness affects processing of binaural spatial cues for sound localization (azimuth) in the auditory cortex. The differences between SC and CB observed here include a reduced BOLD response in left medial auditory cortex of CB, a more robust level-invariance for spatial tuning width in CB, and, most strikingly, a reduced sensitivity to binaural spatial cues in CB. Furthermore, the occipital areas that are activated in CB during sound location processing were not modulated by binaural spatial information either. Our results thus indicate that blind humans may encode sound (azimuth) position employing a different mechanism. Future research is needed to investigate such alternative mechanisms, including the use of monaural, spectral cues.

## References

1. King AJ & Parsons CH (1999) Improved auditory spatial acuity in visually deprived ferrets. *European Journal of Neuroscience* 11(11):3945-3956.
2. Rauschecker JP & Kniepert U (1994) Auditory localization behaviour in visually deprived cats. *European Journal of Neuroscience* 6(1):149-160.
3. Röder B, *et al.* (1999) Improved auditory spatial tuning in blind humans. *Nature* 400(6740):162-166.
4. Voss P, *et al.* (2004) Early- and late-onset blind individuals show supra-normal auditory abilities in far-space. *Current Biology* 14(19):1734-1738.
5. Gougoux F, Zatorre RJ, Lassonde M, Voss P, & Lepore F (2005) A functional neuroimaging study of sound localization: visual cortex activity predicts performance in early-blind individuals. *PLoS Biol* 3(2):e27.
6. Lessard N, Pare M, Lepore F, & Lassonde M (1998) Early-blind human subjects localize sound sources better than sighted subjects. *Nature* 395(6699):278-280.
7. Voss P, Tabry V, & Zatorre RJ (2015) Trade-off in the sound localization abilities of early blind individuals between the horizontal and vertical planes. *The Journal of Neuroscience* 35(15):6051-6056.
8. Weeks R, *et al.* (2000) A positron emission tomographic study of auditory localization in the congenitally blind. *The Journal of Neuroscience* 20(7):2664-2672.
9. Collignon O, *et al.* (2011) Functional specialization for auditory-spatial processing in the occipital cortex of congenitally blind humans. *Proceedings of the National Academy of Sciences* 108(11):4435-4440.
10. Renier LA, *et al.* (2010) Preserved functional specialization for spatial processing in the middle occipital gyrus of the early blind. *Neuron* 68(1):138-148.
11. Elbert T, *et al.* (2002) Expansion of the tonotopic area in the auditory cortex of the blind. *The Journal of Neuroscience* 22(22):9941-9944.
12. Röder B, Rösler F, Hennighausen E, & Näcker F (1996) Event-related potentials during auditory and somatosensory discrimination in sighted and blind human subjects. *Cognitive Brain Research* 4(2):77-93.

13. Stevens AA & Weaver KE (2009) Functional characteristics of auditory cortex in the blind. *Behavioural brain research* 196(1):134-138.
14. Jiang F, Stecker GC, & Fine I (2014) Auditory motion processing after early blindness. *Journal of vision* 14(13):4-4.
15. Dormal G, Rezk M, Yakobov E, Lepore F, & Collignon O (2016) Auditory motion in the sighted and blind: early visual deprivation triggers a large-scale imbalance between auditory and “visual” brain regions. *Neuroimage* 134:630-644.
16. Jiang F, Stecker GC, Boynton GM, & Fine I (2016) Early blindness results in developmental plasticity for auditory motion processing within auditory and occipital cortex. *Frontiers in human neuroscience* 10.
17. Korte M & Rauschecker JP (1993) Auditory spatial tuning of cortical neurons is sharpened in cats with early blindness. *Journal of Neurophysiology* 70(4):1717-1721.
18. Derey K, Valente G, de Gelder B, & Formisano E (2015) Opponent Coding of Sound Location (Azimuth) in Planum Temporale is Robust to Sound-Level Variations. *Cerebral Cortex*:bhw269.
19. Musicant AD & Butler RA (1985) Influence of monaural spectral cues on binaural localization. *The Journal of the Acoustical Society of America* 77(1):202-208.
20. Oldfield SR & Parker SP (1984) Acuity of sound localisation: a topography of auditory space. II. Pinna cues absent. *Perception* 13(5):601-617.
21. Engel SA, Glover GH, & Wandell BA (1997) Retinotopic organization in human visual cortex and the spatial precision of functional MRI. *Cerebral cortex* 7(2):181-192.
22. Striem-Amit E, Hertz U, & Amedi A (2011) Extensive cochleotopic mapping of human auditory cortical fields obtained with phase-encoding fMRI. *PLoS One* 6(3):e17832.
23. Harms MP & Melcher JR (2002) Sound repetition rate in the human auditory pathway: representations in the waveshape and amplitude of fMRI activation. *Journal of Neurophysiology* 88(3):1433-1450.
24. Harms MP & Melcher JR (2003) Detection and quantification of a wide range of fMRI temporal responses using a physiologically-motivated basis set. *Human brain mapping* 20(3):168-183.
25. Mumford JA & Nichols T (2009) Simple group fMRI modeling and inference. *Neuroimage* 47(4):1469-1475.
26. Dale AM (1999) Optimal experimental design for event-related fMRI. *Human brain mapping* 8(2-3):109-114.
27. Lee C-C & Middlebrooks JC (2011) Auditory cortex spatial sensitivity sharpens during task performance. *Nature neuroscience* 14(1):108-114.
28. Brunetti M, *et al.* (2005) Human brain activation during passive listening to sounds from different locations: an fMRI and MEG study. *Human brain mapping* 26(4):251-261.
29. Deouell LY, Heller AS, Malach R, D'Esposito M, & Knight RT (2007) Cerebral Responses to Change in Spatial Location of Unattended Sounds. *Neuron* 55(6):985-996.
30. Warren JD & Griffiths TD (2003) Distinct mechanisms for processing spatial sequences and pitch sequences in the human auditory brain. *The journal of neuroscience* 23(13):5799-5804.
31. van der Zwaag W, Gentile G, Gruetter R, Spierer L, & Clarke S (2011) Where sound position influences sound object representations: A 7-T fMRI study. *NeuroImage* 54(3):1803-1811.
32. Campain R & Minckler J (1976) A note on the gross configurations of the human auditory cortex. *Brain and language* 3(2):318-323.
33. Leonard CM, Puranik C, Kuldau JM, & Lombardino LJ (1998) Normal variation in the frequency and location of human auditory cortex landmarks. Heschl's gyrus: where is it? *Cerebral Cortex* 8(5):397-406.

34. Shapleske J, Rossell SL, Woodruff PWR, & David AS (1999) The planum temporale: a systematic, quantitative review of its structural, functional and clinical significance. *Brain Research Reviews* 29(1):26-49.
35. Manjunath N, *et al.* (1998) Shorter latencies of components of middle latency auditory evoked potentials in congenitally blind compared to normal sighted subjects. *International journal of neuroscience* 95(3-4):173-181.
36. Naito E & Hirose S (2014) Efficient foot motor control by Neymar's brain. *Frontiers in human neuroscience* 8.
37. Jäncke L, Shah N, & Peters M (2000) Cortical activations in primary and secondary motor areas for complex bimanual movements in professional pianists. *Cognitive Brain Research* 10(1):177-183.
38. Koeneke S, Lutz K, Wüstenberg T, & Jäncke L (2004) Long-term training affects cerebellar processing in skilled keyboard players. *Neuroreport* 15(8):1279-1282.
39. Begault DR & Trejo LJ (2000) 3-D sound for virtual reality and multimedia.
40. Carlile S, Martin R, & McAnally K (2005) Spectral information in sound localization. *International review of neurobiology* 70:399-434.
41. Stecker GC, Mickey BJ, Macpherson EA, & Middlebrooks JC (2003) Spatial sensitivity in field PAF of cat auditory cortex. *Journal of neurophysiology* 89(6):2889-2903.
42. Logothetis NK (2008) What we can do and what we cannot do with fMRI. *Nature* 453(7197):869.
43. Epstein RA & Higgins JS (2007) Differential parahippocampal and retrosplenial involvement in three types of visual scene recognition. *Cerebral Cortex* 17(7):1680-1693.
44. Amedi A, Raz N, Pianka P, Malach R, & Zohary E (2003) Early 'visual' cortex activation correlates with superior verbal memory performance in the blind. *Nat Neurosci* 6(7):758-766.
45. Stevens AA, Snodgrass M, Schwartz D, & Weaver K (2007) Preparatory activity in occipital cortex in early blind humans predicts auditory perceptual performance. *The Journal of Neuroscience* 27(40):10734-10741.
46. Tailarach J & Tournoux P (1988) Co-planar stereotaxic atlas of the human brain: 3-dimensional proportional system—an approach to cerebral imaging. *Stuttgart and New York: Thieme Verlag.*
47. Goebel R, Esposito F, & Formisano E (2006) Analysis of functional image analysis contest (FIAC) data with brainvoyager QX: From single-subject to cortically aligned group general linear model analysis and self-organizing group independent component analysis. *Human brain mapping* 27(5):392-401.
48. Kim J-J, *et al.* (2000) An MRI-based parcellation method for the temporal lobe. *Neuroimage* 11(4):271-288.
49. Frost MA & Goebel R (2013) Functionally informed cortex based alignment: an integrated approach for whole-cortex macro-anatomical and ROI-based functional alignment. *Neuroimage* 83:1002-1010.
50. Friston KJ, Frith CD, Turner R, & Frackowiak RS (1995) Characterizing evoked hemodynamics with fMRI. *Neuroimage* 2(2PA):157-165.
51. Middlebrooks JC, Xu L, Eddins AC, & Green DM (1998) Codes for sound-source location in nontopographic auditory cortex. *Journal of Neurophysiology* 80(2):863-881.
52. Stecker GC, Harrington IA, & Middlebrooks JC (2005) Location coding by opponent neural populations in the auditory cortex. *PLoS Biol* 3(3):e78.